

# **THOMSON TUBES ELECTRONIQUES**

## **IMAGE INTENSIFIER DESIGN AND SPECIFICATIONS**

**Dr Paul M. DE GROOT**

**TII/1.087/91**

**SEPTEMBRE 1991**

## IMAGE INTENSIFIER DESIGN AND SPECIFICATIONS

### ABSTRACT

La technologie et la conception de l'intensificateur d'images radiologiques de pointe sont passées en revue. Les principales performances électro-optiques des intensificateurs d'images radiographiques, pertinentes pour une bonne qualité d'image, telles que le facteur de conversion, le DQE, le contraste et la résolution spatiale sont discutées, et leurs méthodes de mesure sont décrites. Certaines applications typiques sont analysées plus en détail, et les tendances futures sont données.

### I. INTRODUCTION

Un intensificateur d'images radiologiques est un appareil qui convertit un motif de rayons X incident en une image de lumière visible correspondante qui peut ensuite être détectée soit sur un film, soit avec une caméra de télévision. Dans une chaîne d'imagerie fluoroscopique ou fluorographique bien conçue, l'intensificateur d'image radiologique, en tant que détecteur frontal, est le composant le plus important. Toute perte d'information d'image ou toute augmentation de bruit survenant à ce premier stade est irréversible, et les caractéristiques des intensificateurs d'image radiologique ont, plus que celles de tout autre composant, un effet déterminant sur la qualité de l'image finale.

Comme les intensificateurs d'images radiographiques fournissent également une amplification significative du signal, leur utilisation a permis de réduire considérablement les débits de dose de rayons X et donc l'exposition des patients. En outre, leur capacité inégalée à fournir des images en temps réel à des vitesses pouvant atteindre plus de 100 images par seconde fait des intensificateurs d'images radiologiques des appareils de choix pour les techniques modernes d'imagerie diagnostique par rayons X, telles que la D.S.A. ou l'angiographie cardiaque.

Les premiers intensificateurs d'images à rayons X sont apparus dans les années 1950 et offraient une qualité d'image nettement inférieure à celle des combinaisons écran-film classiques. Cependant, leurs performances n'ont cessé de s'améliorer depuis, et le contraste et la résolution spatiale se rapprochent désormais de ceux des combinaisons écran-film directes. Une percée majeure a eu lieu dans les années 1960 avec l'introduction du Csl évaporé comme matériau de scintillation. Le Csl a des caractéristiques d'absorption bien adaptées aux spectres de rayons X utilisés en imagerie médicale et la structure en aiguille de la couche évaporée offre une résolution spatiale supérieure à celle d'autres écrans phosphorescents tels que le Gd<sub>2</sub>O<sub>2</sub>S, le ZnCdS ou le CaW<sub>04</sub>.



Les sections suivantes passent en revue la technologie et les performances des intensificateurs d'images à rayons X modernes de pointe. La première partie est consacrée aux caractéristiques physiques des principaux composants à l'intérieur du tube. La deuxième partie décrit les performances d'image des intensificateurs d'images de rayons X et la façon dont leurs paramètres électro-optiques sont définis.

Traduit avec [www.DeepL.com/Translator](http://www.DeepL.com/Translator) (version gratuite)

## II. PHYSICAL CHARACTERISTICS

The typical structure of an X-ray image intensifier is shown in figure 1. It comprises a vacuum bottle with an X-ray transparent input window and a glass or fiber-optic output window through which the output image is displayed. The three principal components inside the bottle are the input scintillator screen on its substrate, the different electrodes that form the electron optics and the output phosphor screen that restores the visible image. The following subsections will describe the physical characteristics of each of these components in more detail.

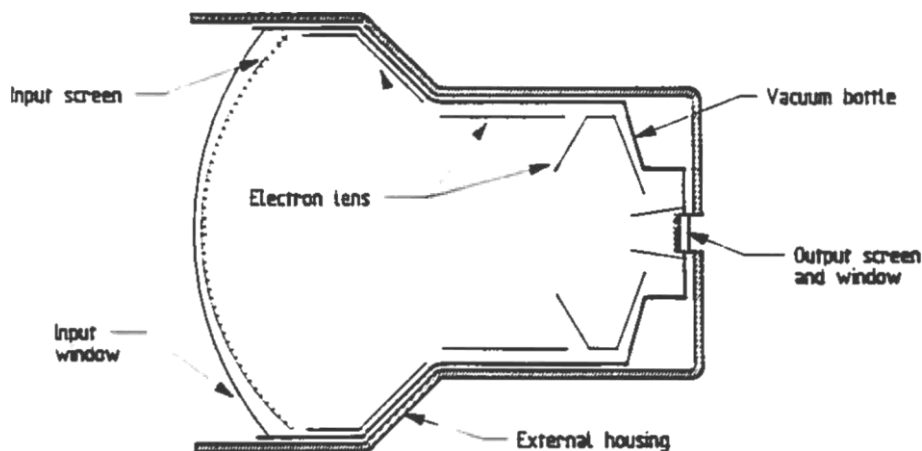


Figure 1 : Typical structure of an X-ray image intensifier.

### II. 1 Input window and scintillator substrate

The input window of the X-ray image intensifier must be vacuum tight and have the highest possible transmission for the incident X-rays. Among the various materials used, such as glass, titanium, steel or aluminum, aluminum offers the best compromise. As a low  $Z$  material it has excellent transmission down to about 35 kVp and produces little scattering of the X-rays. Moreover its convex shape enables the input screen to be brought as close as possible to the entrance plane, thus maximizing the useful entrance field size (see section 111.1). For this reason aluminum has now become the preferred choice for most medical applications.

The thickness of the aluminum input window varies typically from 0.7 to 1.2 mm depending on the size and the type of tube. Despite their small thickness, such convex windows are able to withstand the atmospheric pressure, which in the case of a 40 cm (16") tube represents a weight of more than 1000 kg. Obviously such windows should be handled with great care and never be directly exposed to the patient. A local accidental pressure on such windows may cause them to implode into a concave shape, although generally even in this case the vacuum is not destroyed.

For practical reasons the scintillator material is generally not directly evaporated onto the input window, but on a substrate placed closely behind it. This substrate itself is also made of aluminum with a thickness of about 0.5 mm. Since the substrate is the first element of the multi-electrode electron lens, its shape is precisely calculated to match the rest of the electron optics.

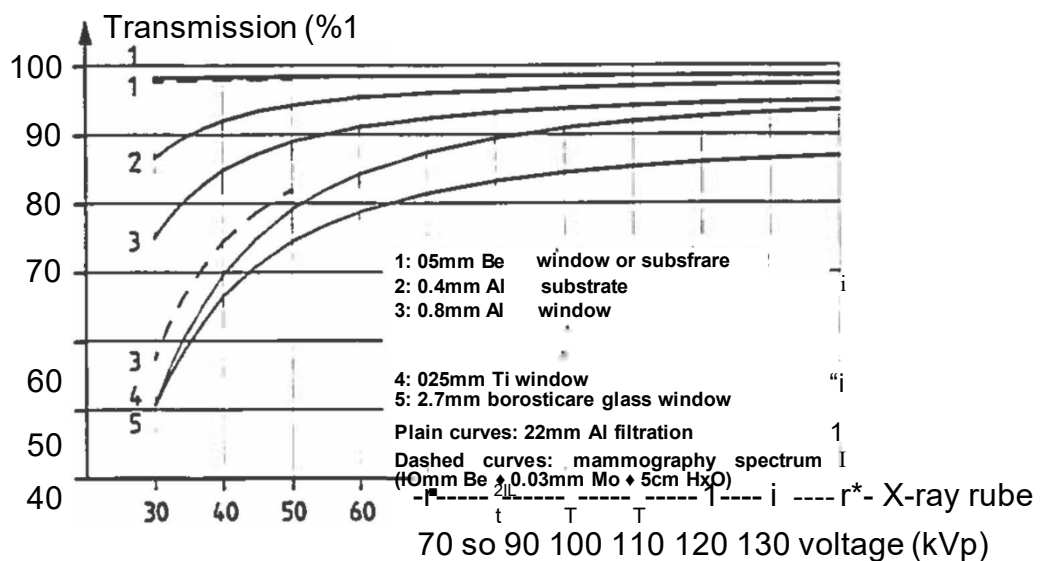


Figure 2 : Useful X-ray transmission of various input windows as a function of X-ray tube voltage.

Figure 2 shows the X-ray transparencies of the scintillator substrate and of various materials used for the input window. The transparencies are calculated for the direct (unscattered) X-rays only. The X-rays scattered in the different media between the X-ray tube and the image tube, which normally are filtered out with an anti-scatter grid, are not taken into account. Two types of filtration are considered : the plain curves correspond to a total filtration of 22 mm of aluminum which is representative for a general case with an adult patient; the dashed curves correspond to a typical mammographic spectrum with a 5 cm breast phantom.

As can be seen, all metallic input windows have transparencies of more than 80 percent above 50 kVp, but show significant absorption at lower energies. Only Be windows remain fully transparent at energies down 30 kVp. Glass input windows produce significant X-ray scatter, which limits their useful transmission even at high kVp.

## II. 2 Input scintillator and photocathode

At the energies used in diagnostic imaging the absorption of X-rays in the scintillator occurs primarily through a mechanism which is called the photoelectric effect. In this process the energy of the absorbed X-ray quantum is entirely absorbed by an atom in the scintillator and a primary electron is ejected. The probability for the photoelectric effect to occur increases as the 4th power of the atomic number and therefore efficient scintillators should contain at least one type of high-Z material.

In most cases the resulting orbital vacancy (generally in the K-shell) is filled by an electron from the outer shells of the atom, which results in the emission of a so called characteristic fluorescent photon. In the case of the commonly used CsI:Na scintillator, both the Cs and the I atoms emit such photons, and their energy lies between 30 and 35 keV. The primary electron, the K-shell fluorescent photon, and generally also some lower energy Auger electrons, carry off all the energy of the incident X-ray photon and produce an avalanche of secondary electrons, most of which recombine under the emission of light. The wavelength of this light obviously depends on the scintillator and doping materials

- used, and for CsI:Na the peak wavelength is about 420 nm.

The bandgap of CsI is about 6 eV and by analogy with well known semiconductors such as Si one might assume that the creation of an electron-hole pair requires an energy of about 20 eV. A typical X-ray quantum of 60 keV would therefore produce a light pulse of about 3000 photons.

The major portion of the light reaches the rear (inner) surface of the scintillator onto which a thin semitransparent photocathode is evaporated. These multialkaline photocathodes contain a mixture of antimony and various alkali metals and have a sensitivity which is matched to the wavelength of the emitted light. Typically 10 to 20 percent of the light photons reaching the photocathode produce photoelectrons which subsequently are accelerated by the electron optics towards the output screen. The total number of photoelectrons produced depends on the energy of the impinging X-rays and is typically about 400 for an incident X-ray quantum of 60 KeV.

The ideal scintillator should absorb all the incident X-rays and convert them into light with the highest possible efficiency. High absorption of X-rays can be achieved by increasing the thickness of the scintillating layer. This, however, also increases the lateral diffusion of the light inside the layer and consequently reduces its spatial resolution.

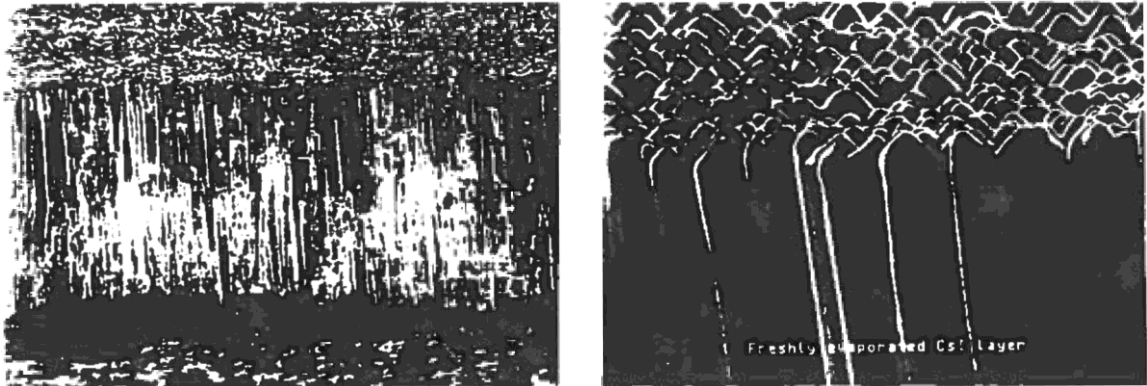


Figure 3 : SEM photograph of a freshly evaporated CsI layer on its substrate (left) and a magnified view of the needle structure (right).

State-of-the-art X-ray image intensifiers almost exclusively use evaporated cesium iodide layers as the scintillator material because of their needle, "fiber optic like" structure (see figure 3). This structure limits the lateral diffusion of light, and for a given X-ray absorption efficiency, CsI layers provide better resolution than any other type of scintillator. However, even with this material the optimum thickness is generally a compromise between high absorption efficiency and good resolution. Depending on the tube type and technology used, the thickness of the CsI layers today typically vary between 300 and 450  $\mu\text{m}$ .

The diameter of the individual needles just after evaporation is very small (about 5  $\mu\text{m}$ ), but during the subsequent heat treatments some coalescence between the needles generally occurs. The relative density of the evaporated layers varies typically between 80 and 90 percent of the bulk material which is about twice as high as the relative density of  $\text{Gd}_2\text{O}_2\text{S}$  or  $\text{CaWO}_4$  screens. Its final structure depends in a very sensitive way on the evaporation conditions (speed, temperature, geometry etc.) and the subsequent heat treatments, and essentially determines the electro-optical characteristics of the layer.

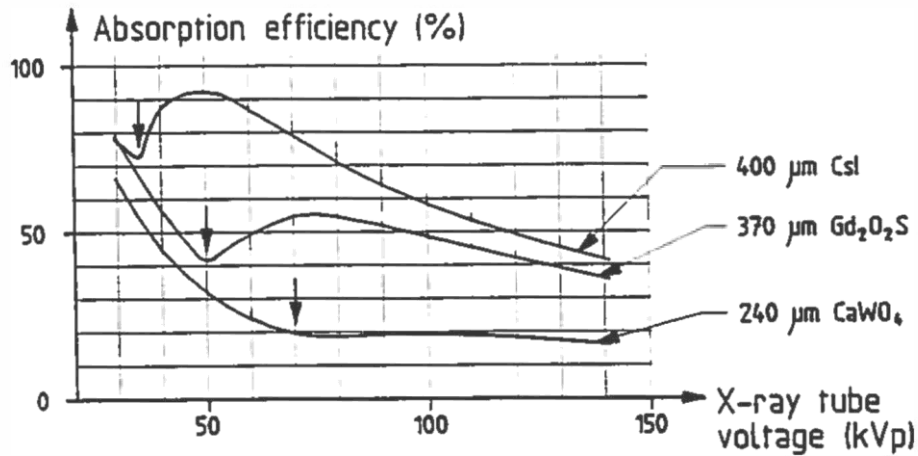


Figure 4 : Useful energy absorption efficiencies of frequently used scintillator screens. The CaWO<sub>4</sub> and Gd<sub>2</sub>O<sub>2</sub>S curves refer to screen pairs, and the relative densities for CsI, CaWO<sub>4</sub> and Gd<sub>2</sub>O<sub>2</sub>S are assumed to be 0.85, 0.40 and 0.43 respectively.

Figure 4 shows a comparison of the energy absorption efficiency of a typical CsI screen with medium speed CaWO<sub>4</sub> and Gd<sub>2</sub>O<sub>2</sub>S screens as a function of the X-ray tube voltage. The characteristic K-absorption edges of these screens are indicated by arrows. The curves are calculated for a 25 cm H<sub>2</sub>O phantom and do not take into account the scattered X-rays ; i.e. only the useful absorption is considered. As can be seen, CsI screens have absorption characteristics which are superior to the other screens over the whole practical range of X-ray spectra.

## II. 3 Electron Optics

The electron optics ensure that the photoelectrons emitted by the photocathode are correctly focused on the output phosphor screen. Moreover the accelerating field experienced by the electrons along their trajectories provides a powerful and virtually noise free gain mechanism which bestows X-ray image intensifiers with unequalled performances in gain and signal-to-noise ratio compared to direct screen-film combinations (see section III. 2).

The ideal electron optics should focus the photoelectronic image emitted from the curved input screen onto the generally flat output screen without any distortion or loss of resolution. Of course such a structure does not exist, and a compromise has to be found between the complexity of the structure (the number of electrodes), the uniformity of resolution, the distortion and the tube length. The mechanical constraints of diagnostic equipment, for example, require the shortest possible length of the tube but this, in turn, requires more curvature of the input screen which increases the distortion (see section 111.7).

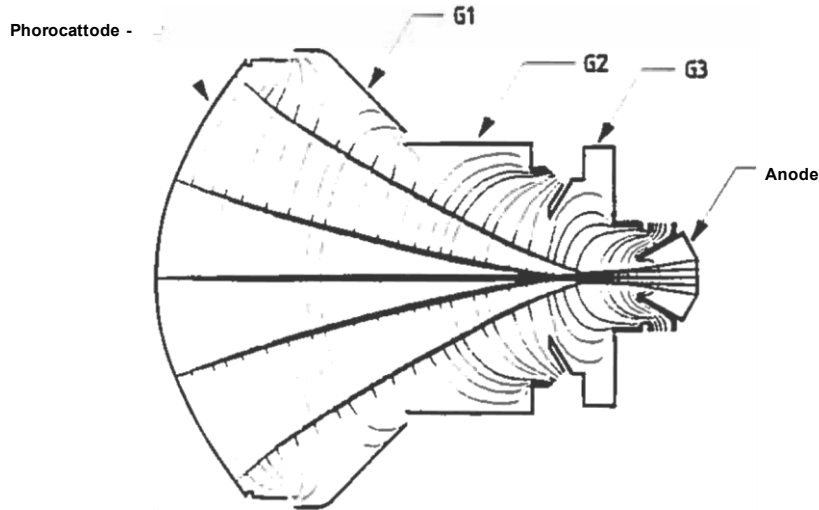


Figure 5 : Electron optics of 9 typical pentode structure showing the electron trajectories and the isopotential curves.

A very common design is the so called pentode structure (see figure 5) in which three additional electrodes (G1, G2 and G3) are inserted between the photocathode, generally at zero potential and the output screen which is at a high positive potential (typically 30 kV). The G3 electrode allows one to zoom the image by varying the portion of the input screen that is projected onto the output screen : the higher the G3 voltage, the smaller the portion of the input screen that is projected, i.e. the larger the magnification. The G2 electrode is the focussing electrode, and the G1 electrode permits one to adjust the resolution uniformity throughout the whole image field.

Figure 5 shows the electron trajectories and isopotential curves for a typical structure. The field strength is the largest at the interspaces between G2 and G3 and between G3 and anode. Therefore the electrode surfaces in these zones have to be prepared with great care ; otherwise spurious emission of electrons will produce undesirable glow or flicker in the image.

The electron optical MTF depends mainly on the initial spread in energy and direction of the photoelectrons just after emission from the photocathode. By increasing all electrode voltages by the same factor this lateral spread of the electrons can be reduced and hence the MTF improved. This however requires more stringent conditions on the insulation of the electrodes inside and outside the tube, and most X-ray image intensifiers operate with a cathode to anode voltage in the 25 to 35 kV range.



## II. 4 Output screen

The output screen converts the energy of the impinging electrons into light and thus restores the original X-ray image as a visible image that can be projected either on film or on a television camera.

In order to achieve efficient optical coupling between the image tube and the collimation lens the diameter of the output screen is generally made much smaller than the input screen (typically between 15 and 35 mm). Since all the image information is now concentrated on a much smaller area, the output phosphor should have a very fine grain with low fixed pattern noise.

The output screen consists of a thin layer of small phosphor particles. Because of its high light yield and its fast response, most image intensifiers use P20 as the phosphor material. The P20 phosphor is a mixture of zinc cadmium sulphide doped with silver ( $Zn_{0.8}Cd_{0.4}S:Ag$ ) which emits in the green portion of the spectrum with a peak wavelength between 520 and 540 nm. This matches well with the sensitivity curves of high quality orthochromatic films and most of the photoconductive detectors used in television cameras.

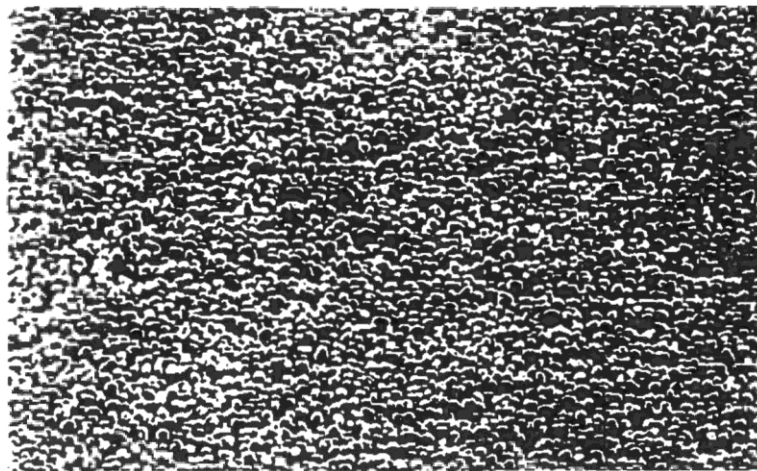


Figure 6 : SEM photograph of a P20 output phosphor screen.

The typical size of the P20 phosphor particles is between 1 and 2  $\mu m$  and the total thickness of the layer generally varies between 4 and 8  $\mu m$ .

Figure 6 shows an electron microscopic view of a P20 output screen deposited on its substrate. The vacuum side of the screen is covered with a thin aluminum film (not shown) of typically 200 to 300 nm thickness to which the anode voltage is applied. At these thicknesses the transmission of the aluminum film for the impinging electrons exceeds 90 %.

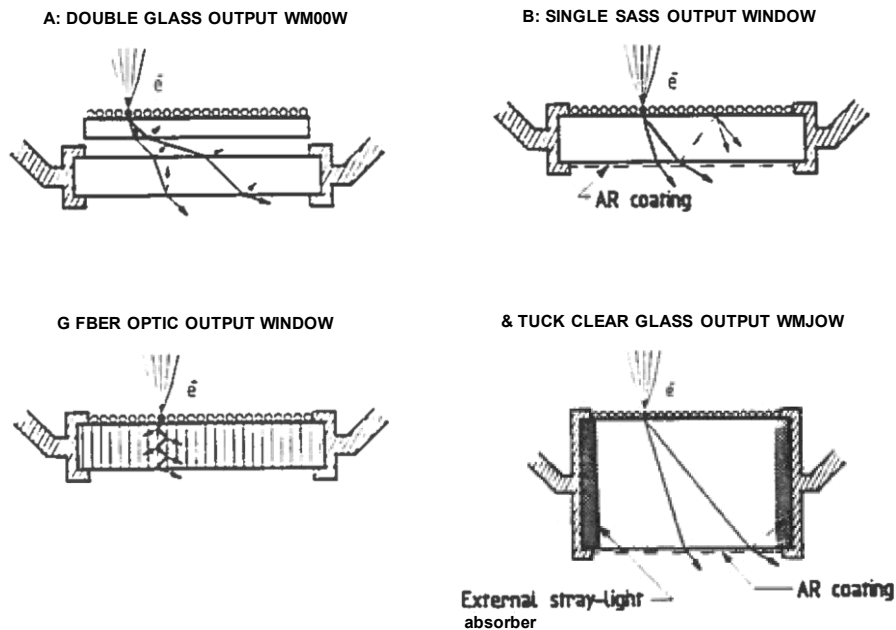
Typically at an incident energy of 30 kV, each impinging electron causes the emission of around 1000 light photons at the window side of the output screen.



## II. 5 Output window

The output window of the X-ray image intensifier must be vacuum tight and must have a good transmission for the light emitted by the phosphor. Currently used output window structures are shown in figure 7.

The various figures show how the light is originated at a given point of the screen by the focussed electron beam and how this light is subsequently transmitted and reflected at the various interfaces of the output window.



Agure 7 : Frequently used output window structures.

\* Structure A is a conventional double glass output window, where the phosphor screen is deposited on a substrate (upper part) which is physically separated from the glass window (lower part) that ensures the vacuum tightness.

This structure produces a relatively large amount of veiling glare due to the multiple reflections of the light at the various interfaces.

\* Structure B is a single glass output window with the phosphor layer deposited directly on it. These structures generally also have an antireflection coating at the outer surface which eliminates all reflections at low angles. Only light emitted at larger angles continues to be reflected and produces some veiling glare.

Both structures A and B generally employ a semitransparent glass with a transmission  $T$  between 0.6 and 0.8 in order to attenuate the veiling glare produced by the reflected light.



Indeed the veiling glare arises from rays that exit the output window after at least 3 internal reflections and therefore are attenuated by a factor of at least  $T^3$ . Since the direct light beam is only attenuated by a factor  $T$ , the ratio of the direct light to the veiling glare, which determines the contrast ratio is improved by a factor of  $1/T^2$ .

Naturally, the disadvantage of such structures is the attenuation of the light output (and hence the gain) of the image tube by a factor  $T$  compared to fully transparent glass windows.

\* Structure C is a fiber-optic window, consisting of an array of very small fibers with a diameter of typically 5 to 10  $\mu$ . Since the light remains channelized in these fibers the image originated in the output phosphor is directly transposed to the opposite surface and, unlike glass windows, fiber optic windows require the lens to be focussed on the outer surface.

Because of the "light channeling" effect inside the fibers, lateral light diffusion is also greatly reduced, although not completely eliminated. Indeed a fraction of the light may escape from their original fibers and diffuse laterally before entering other fibers, thus lowering the contrast. Fiber-optic output windows also have a limited optical transmission of typically 0.5 to 0.8. Unlike plain glass windows which do not cause any image degradation, fiber-optic output windows do cause some loss in spatial resolution and may present characteristic cosmetic defects like "chicken wire", shear distortion or dead fibers.

An interesting feature of fiber-optic windows is that they allow for direct fiber-optic coupling with the T.V. detector like a pick-up tube or a CCD. This provides a gain in volume compared to conventional coupling through lenses, but is however only possible in single port systems (TV only) and excludes the use of photospot or cine cameras.

\* Structure D shows a very thick plain clear glass output window. Such windows have recently made their appearance and combine the advantages of both excellent transmission (close to 100 percent) and very high contrast. The glass thickness is typically 14 mm or more, which is about 4 to 5 times the thickness used in conventional glass output windows.

As the figure shows, at large angles of emission the light continues to be reflected at the outer surfaces, but then strikes the cylindrical wall instead of reaching the output screen again like in structure B. If the periphery of the window is adequately treated with an absorbing glass these reflected rays are completely absorbed, and consequently such windows are virtually free of veiling glare and show excellent contrast without any of the disadvantages of the previous structures. Of course these output windows need to be coupled with lenses that have been especially designed for such a large glass thickness; otherwise serious deterioration of the resolution of the total system will occur. Recently several lenses of various focal lengths have become available, which perfectly match these new type output windows.



III. ELECTRO OPTICAL CHARACTERISTICS

III. 1. Entrance field size

X-ray image intensifiers are available with a large variety of field sizes, ranging from 10 cm (4") to 57 cm (22"). Most medical examinations however are carried out with field sizes between 15 cm (6") and 40 cm (16").

The entrance field size of an X-ray image intensifier is specified either by the nominal or by the useful entrance field diameter. The difference between these two parameters is explained in figure 8. The entrance field size is defined in the entrance plane which, in turn, is defined as the plane perpendicular to the principal axis of symmetry of the X-ray image intensifier and barely touching its most protruding part in the direction of the X-ray source. When the image intensifier is irradiated with a parallel X-ray beam it can be seen from the figure that the output image corresponds to an entrance field size given by  $\phi_N$  the nominal entrance field diameter.

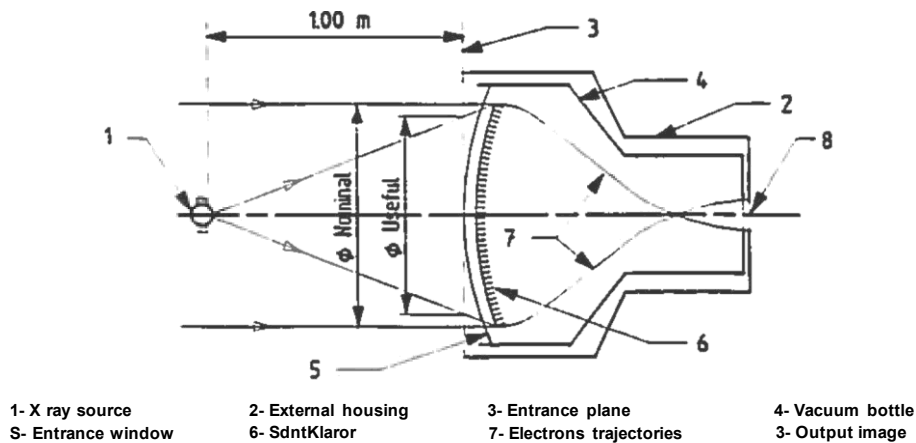


Figure 8 : Definition of nominal and useful entrance field diameter.

Since however a parallel X-ray beam is never achieved in practical situations (it would require the X-ray source to be placed at infinity), a second parameter is more commonly used : the useful entrance field diameter  $\phi_U$  corresponds to that area in the entrance plan which is visualized in the output image, when the source to entrance plane distance (S.E.D.) is exactly 1.00 meter (IEC 520).

$\phi_U$  is always smaller than  $\phi_N$  but the relationship between both diameters is not unambiguously defined and depends on the curvature of the input screen and its distance from the entrance plane. Figure 9 shows examples of tubes having all the same nominal entrance fields, but different useful field sizes : figure A shows the influence of the input screen curvature on the useful entrance field, and figure B the influence of its distance to the entrance plane.

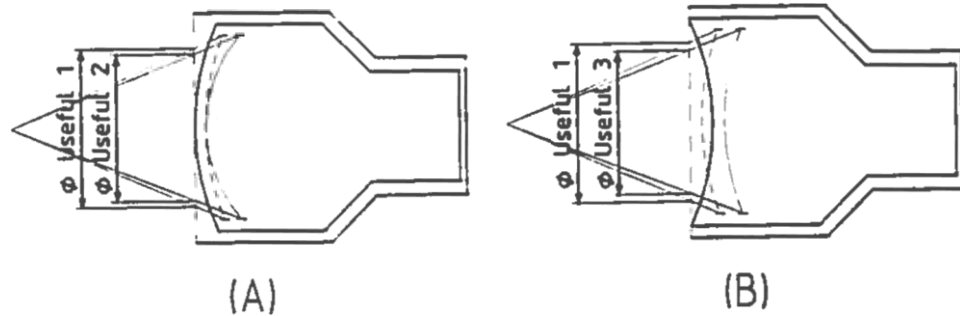


Figure 9 : Influence of the input screen curvature (left) and position (right) on the useful entrance field diameter.

From the above figure it becomes clear that for given outer dimensions of the X-ray image intensifier, the maximum useful entrance field is obtained by placing the scintillator as close as possible to the entrance plane and by shaping it as flat as possible. This precludes concave type input windows, and today most image intensifiers possess a convex type input window, generally made of aluminum.

For a given structure, the entrance field obviously depends on the S.E.D. and approaches the nominal value at large distances. Figure 10 shows the exact dependence of the entrance field size on the S.E.D. for some commonly used field sizes. The values at 1.00 meter correspond to the useful entrance field size as defined in IEC 520.

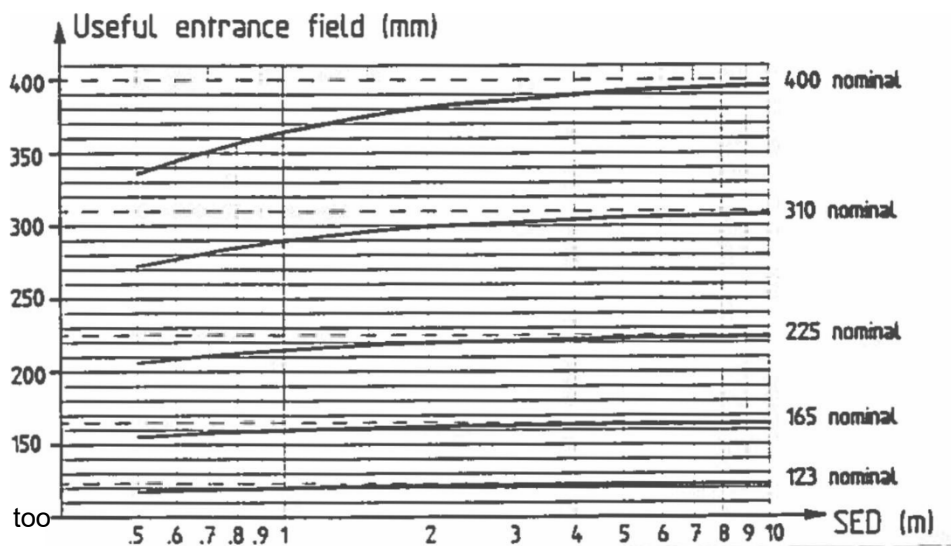


Figure 10 : Variation of the useful entrance field as a function of the source-to-entrance plane distance (SED) for various field sizes.



Because of the geometrical magnification between the patient and the image intensifier, the visible area at the patient level is still smaller than the useful entrance field diameter itself. Table 1 summarizes for various field sizes, the relationship between the nominal and useful entrance field as well as the visible field at the patient level taken at 30 cm from the entrance plane.

Nominal entrance field (mm)	Useful entrance field (mm)	Visible patient field (mm)
400 (15.7")	365 (14.4")	255 (10")
355 (14.0")	330 (13.0")	230 (9.0")
310 (12.2")	290 (11.4")	203 (8.0")
225 (8.9")	215 (8.5")	150 (5.9")
165 (6.5")	160 (6.3")	112 (4.4")
123 (4.8")	120 (4.7")	84 (3.3")

Table 1 : Relationship between different field sizes. The visible field at the patient level is taken at 30 cm from the entrance plane.

III. 2 Conversion factor

As its name indicates, the primary function of an X-ray image intensifier is to convert and amplify the signal, and hence its gain is of great importance. The gain is generally referred to as the conversion factor and is defined as the ratio of the output light flux or luminance to the incident X-ray exposure rate. Frequently used units for the output luminance are  $cd\ m^{-2}$  or ftL, and exposure rates are generally expressed in  $mRs^{-1}$ ,  $//Gys^{-1}$  or  $pCkg^{-1}s^{-1}$ . Table 2 can be used to convert between the different units.

	$cdm^2/mRs^{-1}$	$cdm^2//Gy^{-1}$	$cdm^2/j/Ckg^{-1}s^{-1}$	ftL/mRs <sup>-1</sup>
1 $cdm^2/mRs^{-1}$ =	1	0,115	3,88	0,292
1 $cdm^2//Gys^{-1}$ =	8,7	1	33,8	2,54
1 $cdm^2/z/Ckg^{-1}s^{-1}$ =	0,258	0,0296	1	0,0753
1 ftL/mRs <sup>-1</sup> =	3,43	0,394	13,3	1

Table 2 : Conversion table between the various units used to express the conversion factor.

Since the output luminance is a flux density, the conversion factor of an X-ray image intensifier depends not only on the yields of the various transmission and conversion processes inside the tube (the intrinsic gain), but also on the ratio of the output image size to the entrance field size (the demagnification ratio).

The intrinsic gain (defined as the ratio of the total amount of light emitted to the total amount of radiation received) depends only on the nature and the quality of the materials used, such as the absorption efficiency of the scintillator, the sensitivity of the photocathode, the luminous efficiency of the output phosphor, or the transmission of the input and output windows. Because of the high acceleration fields used inside the tube, the intrinsic gain of X-ray image intensifier is at least a hundred times larger than the intrinsic gain of conventional screens used in direct radiography. Typically each absorbed X-ray photon produces on the average about  $3 \cdot 10^5$  light photons at the output window compared to about 1500 for a rare-earth direct screen.

The demagnification ratio on many X-ray image intensifiers is about 10 in the normal mode of operation, which provides an additional gain of about 100 in the light output flux density (i.e. the luminance) compared to a 1:1 imaging ratio.

Naturally this additional increase of a factor of 100 in the conversion factor due to the demagnification ratio does not mean that the gain of the total system is increased by the same amount. This is illustrated in the following example :

Let us compare two image intensifiers which are exactly identical except for the output image diameter : for example tube A has a 20 mm and tube B a 25 mm output image. For the same total photo-electric current on the output screen tube B will have an output luminance, and consequently a conversion factor, which is  $(20/25)^2 = 0.64$  times that of tube A. However the total amount of light integrated over the whole surface will be the same and, provided that in both cases a tandem lens with the same aperture is used, the illumination level on the image detector (film, TV camera) also remains unchanged. Therefore, despite the lower conversion factor of the tube B, the overall gain of the X-ray image intensifier system in the above example remains unchanged.

In order to keep the same image size on the film or TV camera, tube B will however require a collimator lens with a focal length 1.25 times longer than that of tube A, and therefore the diameter of lens B should also be 1.25 times larger. Of course such a lens would be more cumbersome and for these reasons the relative aperture (f/D ratio) of lenses generally decreases with their focal length.

Thus the overall gain (defined as the ratio of the illumination level on the image detector to the the entrance field exposure rate) of the system will generally decrease with increasing output image diameter of the image intensifier, but not so much because of the decrease of the conversion factor but because of the lower light collection efficiency of the tandem lens.



The conversion factor also depends on the quality of the incident radiation. The IEC standard 573 specifies that the incident radiation shall have a total filtration equivalent to 22 mm of aluminum and a 1st HVL of 7.0 mm of aluminum, which corresponds to an X-ray tube voltage of about 75 kVp. This filtration was chosen because it produces approximately the same spectrum as 25 cm of water which is representative of an adult patient.

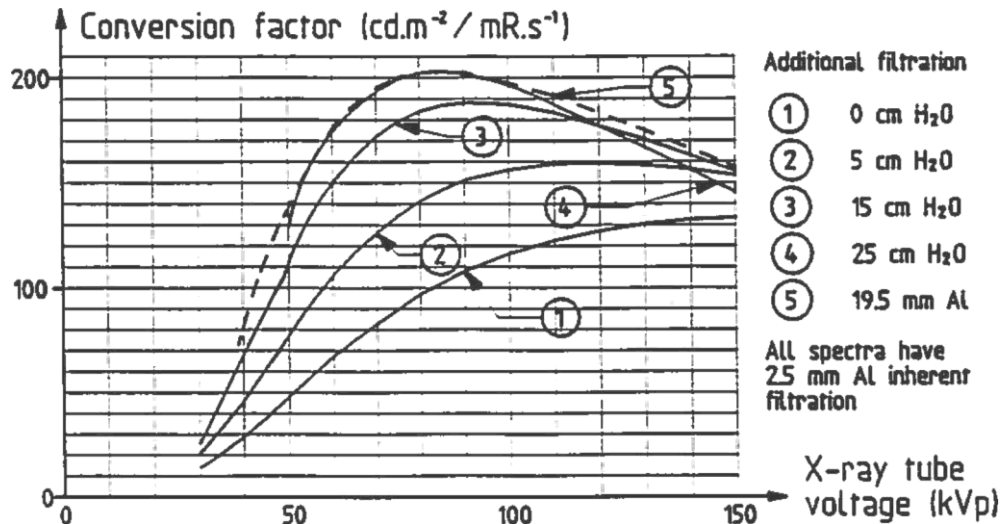


Figure 11 : Variation of the conversion factor with X-ray tube voltage for different patient filtrations.

The variation of the conversion factor with the X-ray tube voltage is shown in figure 11 for different thicknesses of water. The curves are normalized at 200  $\text{cdm}^2/\text{mRs}''$  for standard IEC radiation and are calculated for a CsI layer thickness of 390 //m. An intrinsic filtration of 2.5 Al is assumed. Only direct, unscattered, X-ray photons are taken into account.

Figure 12 shows the ratio of the output luminance of a typical image intensifier to the load current of the X-ray tube as a function of kVp for various water phantoms under the same conditions. At fixed mA the light output depends very strongly on both the kVp setting and the thickness of the water phantom. The light output with 22 mm of Al total filtration is also shown for comparison. Although 22 mm of Al produces an equivalent spectrum (in shape) to that produced by 25 cm of water, it produces a light output which is about 50 times higher.

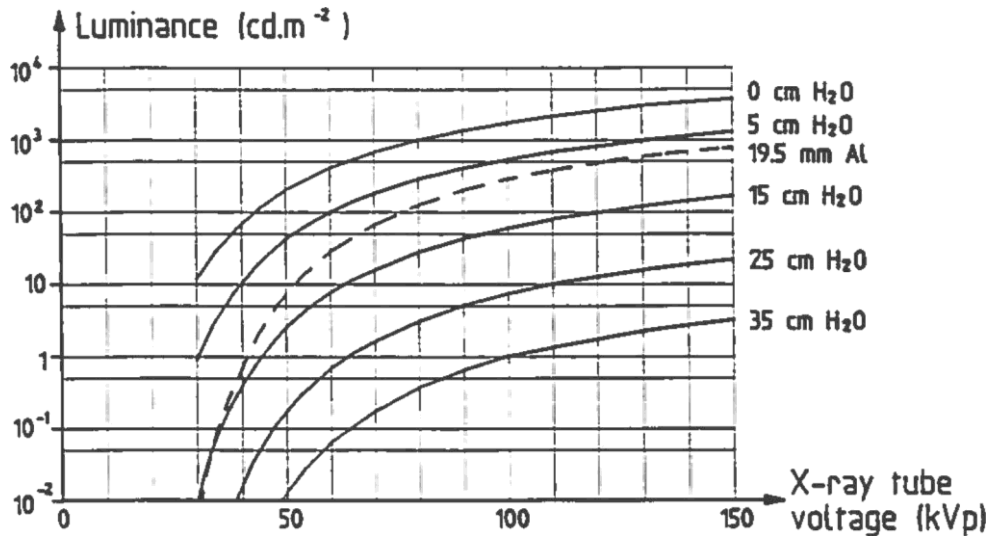


Figure 12 : Typical variation of the output luminance with X-ray tube voltage for 1 mA load current and for various patient filtrations.

Since the optimum value of the output luminance depends on the type of the image detector used (sensitivity of the film or the TV camera) as well as the light collection efficiency of the lenses, it becomes clear that there is no ideal value of the conversion factor which is optimal for applications.

Typically the conversion factor of state-of-the-art X image intensifiers varies between 100 and 400  $\text{cdm}^2/\text{mRs}$ . In most cases a conversion factor between 100 and 200  $\text{cdm}^2/\text{mRs}$  is sufficient and higher values are only required if the magnifying modes are used.

Three different practical applications will now be illustrated in more detail :

\* Standard fluoroscopy with a 9" image intensifier (20 mm output image)

Fluoroscopic examinations may last for relatively long times and therefore patient exposure rates have to be kept as low as possible. During a typical fluoroscopic examination the exposure rate at the entrance of the image intensifier is in the 30 to 60  $\text{pRs}^{-1}$  range. The lower limit is given by the increasing quantum noise level at lower exposure rates (see section III.3).

On the other hand TV detectors require a certain level of illumination in order to operate with a sufficient signal to noise ratio. Table 3 below gives the input illumination of P20 type light that is required for different TV detectors in order to obtain a video output signal - to-noise ratio of about 40 dB.



TV DETECTOR	Illumination for 40 dB SNR
Primicon Plumbicon Saticon	0.8 - 1.0 lux
Standard Sb <sub>2</sub> S <sub>3</sub> vidicon	0.5 - 0.8 lux
2/3" CCD (450.000 pixels)	0.4 - 0.5 lux
Newvicon Chainicon	0.3 - 0.5 lux

Table 3 : Typical sensitivities of TV detectors for P20 light.

The image diameter on the TV detector is typically 15 mm, which requires a tandem lens with a magnification ratio of about 0.75. When widely opened (F/1.4) such a lens system has a collection efficiency E / L of about 8 percent, where E is the illumination in the image plane (TV detector) and L is the output luminance of the image intensifier.

From this and the values in the above table the required output luminance is determined to be between 1 and 4 cdm<sup>2</sup>, and with an entrance dose rate of 30 pRs<sup>-1</sup> the required conversion factor in this example will be between 30 and 130 cdm<sup>2</sup>/mRs<sup>-1</sup> in the normal mode of operation.

\* Cine fluorography with a 9" image intensifier (25 mm output image)

Cine fluorographic sequences typically last between 5 to 10 sec and require higher dose rates in order to keep the quantum noise at a low level. Typical entrance dose rates are between 10 and 15 pR per frame in the 9" mode and between 20 and 25 pR per frame in the 6" mode.

The amount of P20 type light necessary to sensitize a cine film varies from about 0.05 lux.s for a fast film to about 0.20 lux.s for a slow film. The cine image diameter is typically about 25 mm which requires a unity magnification ratio. With a typical lens aperture of F/4.0 this is equivalent to a light output pulse from the image intensifier of 1 to 4 cdm<sup>2</sup>s per cine frame, with 2 cdm<sup>2</sup>s being an average value.

From this it follows that cine fluorographic examinations generally require a conversion factor of at least 150 to 200 cdm<sup>2</sup>/mRs<sup>-1</sup> i.e. several times larger than those necessary in conventional fluoroscopy.



## \* D.S.A.

Digital subtraction angiography (D.S.A) requires the highest possible image quality. In particular the quantum noise, which adds quadratically in the subtracted images should be kept as low as possible, and therefore very high entrance doses of typically 1 to 2 mR per frame are used. In D.S.A. TV pick-up tubes are used in the pulsed progressive mode and require an input light pulse of about 0.3 lux.s for maximum video signal-to-noise ratio (about 60 dB). On the other hand a 1 mR pulse will produce a light output pulse of at least 100 cdm<sup>2</sup>.s and therefore the lenses have to be almost completely closed down (or filtered with optical densities), in order to avoid saturation of the pick-up tube.

The three above examples give a good illustration of the different requirements for the conversion factor of image intensifiers in diagnostic imaging. The highest conversion factor is required in cine fluorography and the lowest in D.S.A.

### 111.3 Detection Quantum Efficiency

The detection quantum efficiency (DQE) provides a measurement for the degradation of the signal-to-noise ratio in the output image ( $SNR_{0U1}$ ) compared to the signal-to-noise ratio of the impinging X-ray beam ( $SNR_{in}$ ). The principal source of noise in the X-ray beam are the statistical quantum fluctuations in the photon flux.

This quantum noise obeys the Poisson statistics and the standard deviation (i.e. the noise) in the photon flux is equal to the square root of its the average value (i.e. the signal). Thus the input signal-to-noise ratio increases as the square root of the number of X-ray quanta and therefore is proportional to the square root of the entrance dose rate.

A perfect imaging chain would add no further noise to this quantum noise and the signal-to-noise ratio in the final image ( $SNR_{inw(J)}$ ) would be equal to  $SNR_{in}$ . In practice however the system always adds some noise and  $SNR_{imao}$  is always smaller than  $SNR_{in}$ . In a well optimized imaging chain the noise contribution of the video chain is relatively small, and the main degradation of the signal-to-noise ratio occurs in the image intensifier itself. This degradation is described by the DQE and defined as  $DQE = SNR_{0U1}^2 / SNR_{in}^2$ .

The principal causes of this degradation inside the image intensifier are the incomplete absorption of the X-ray quanta in the scintillating layer and the statistical fluctuations in the energy conversion process. These processes will now be analyzed in more detail.

\* Absorption process

Let us suppose that on the average  $N$  X-ray photons arrive on a given pixel size in the entrance plane per given time interval. Poisson statistics tells us that the statistical fluctuations in time (i.e. the noise) at the arrival rate will be  $N^{1/2}$  and thus the signal to noise ratio will be  $N/N^{1/2} = N^{1/2}$ . If only a fraction  $A_Q$  of these incoming photons is really absorbed (the other ones passing through without interaction) the number of detected quanta will be  $A_Q \cdot N$ . Since Poisson statistics remain valid the signal-to-noise ratio of the detected photons will be  $A_Q^{1/2} \cdot N^{1/2}$ . Thus  $SNR_{in}^2$  is degraded by a factor equal to the absorption efficiency  $A_Q$ .

◆ Scintillation process

Those X-ray photons that are absorbed will produce an avalanche of light photons (see section 11.2). This multiplication process will also undergo statistical fluctuations which further degrade the signal-to-noise ratio.

Figure 13 shows the pulse height spectrum of the light output from a thick, fully absorbing well-type NaI:Tl reference crystal when irradiated with monochromatic X-rays (59.5 keV) from an  $Am^{241}$  source (left), and a similar spectrum, as recorded from the output of an image intensifier with a CsI:Na input screen of about 400 *fjm* thickness (right).

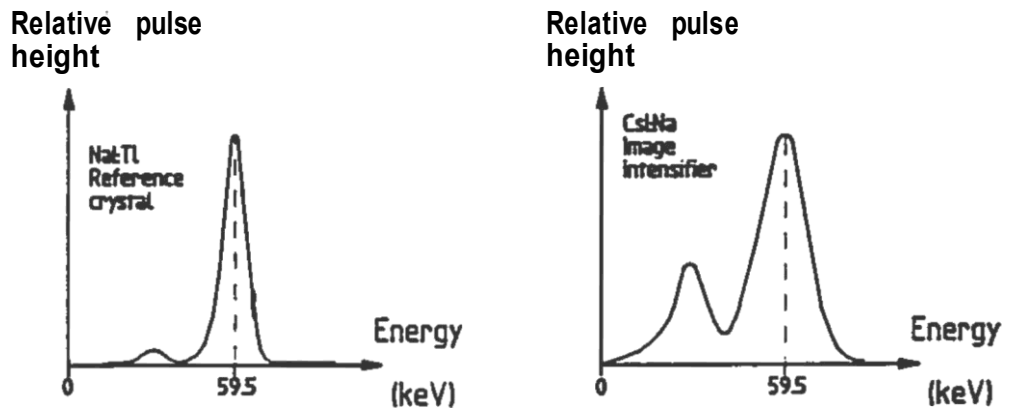


Figure 13 : Pulse height spectra of a fully absorbing NaI:Tl reference crystal (left) and a typical image intensifier (right).

The main peak at 59.5 keV corresponds to the average number of photons which are produced when the energy of the X-ray quantum is completely absorbed inside the scintillator. The width of the peak is due to the natural statistical fluctuations in the scintillation process.



The second peak at lower energies is due to the escape of K-shell fluorescence photons (see section 11.2). Indeed a fraction of these K-shell photons may reescape from the scintillator. In this case only an energy of 59.5 keV less the energy of the escaped K-shell photon will be available for the scintillation process, thus giving rise to a second peak at lower energy.

For the thick NaI:TI crystal the so called escape peak is very small, which shows that only very small fraction of the K-shell photons succeed in escaping from the crystal. In the case of the CsI:Na layer the escape peak is much higher. This is expected since the K-shell photons now have a much higher probability to escape (at both sides) from the thin layer before getting reabsorbed.

The natural width of each peak is also larger for the layer than for the bulk crystal. This is due to the many crystalline and optical non-uniformities in the layer compared to a perfect single crystal.

The total degradation of  $SNR_{in}^2$  produced by these fluctuations in the scintillation process can be shown to be equal to  $A_s = MZ/MQMJ$ , where  $M_0$ ,  $M$ , and  $M_2$  are the different moments of the pulse height distribution.

### Measurement of the detection quantum efficiency

#### A. Recommended method

Once the absorption efficiency  $A_Q$  and the scintillation factor  $A_s$  are known, the DQE is directly determined by  $DQE = A_Q \cdot A_s$ . Modern pulse height counting equipment is commercially available that enables one to measure both  $A_Q$  and  $A_s$  independently with great precision. The absorption efficiency is measured by placing a small radioactive source (typically  $Am^{241}$ ) in front of the image intensifier and counting the number  $N$ , of light pulses produced in the output image. By replacing the image tube with a thick fully absorbing reference crystal, the number  $N_0$  of the impinging X-rays can be found, and  $A_Q$  is directly obtained by  $A_Q = N/N_0$ . The pulse height spectrum is obtained by recording the light output pulses from the image intensifier with a multi-channel analyzer.

Because of its excellent reproducibility and, most importantly, its independence of the temporal lag of the phosphor screens, this so called pulse counting method should preferably be used for DQE measurements, and an IEC standard recommending this method is under preparation.

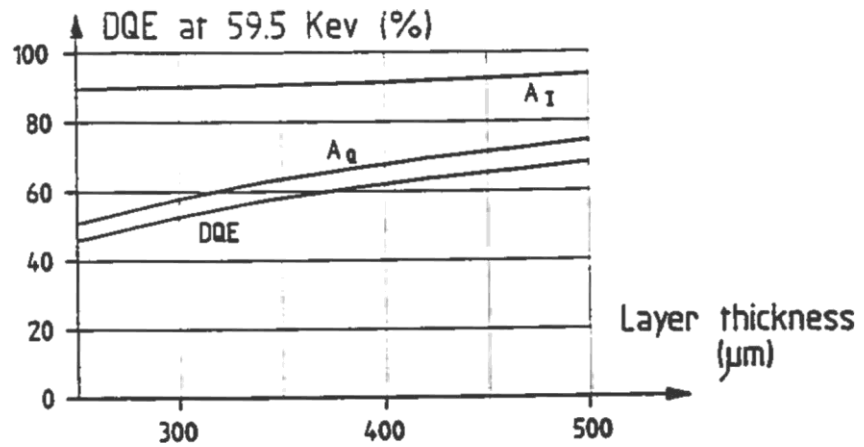


Figure 14 : Variation of DQE with the thickness of the CsI layer.  
 $A_0$  is the quantum absorption efficiency and  $A_I$  represents the signal-to-noise degradation in the scintillation process.

Figure 14 shows the measured DQE at 59.5 keV as a function of the thickness of the CsI layer. An 85 percent packing density is assumed and the measurements were done on an image intensifier with an aluminum window and aluminum scintillator substrate (see figure 2).

As can be seen the scintillation factor  $A_I$  varies only slightly with the thickness, and the thickness dependence of the DQE is mainly determined by the absorption efficiency  $A_0$ .

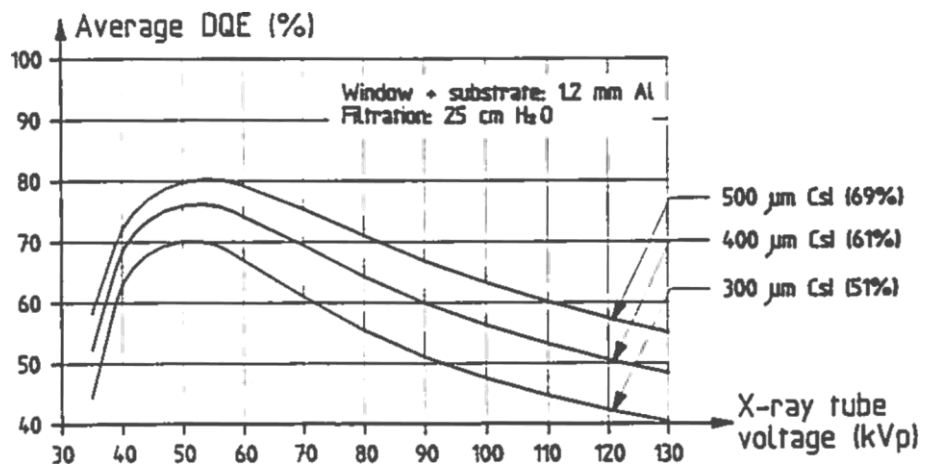


Figure 15 : Variation of the averaged DQE with X-ray tube voltage and with 25 cm of H<sub>2</sub>O filtration for different values of the CsI layer thickness. The values in parentheses give the DQE at 59.5 keV. Relative density of CsI : 0.85.

Figure 15 shows the calculated variation of the average DQE with a 25 cm H<sub>2</sub>O phantom as a function of the X-ray tube voltage for different values of the layer thickness. An aluminum input window and substrate are assumed. The monochromatic DQE at 59.5 keV of each layer is also indicated. It should be noticed that the average DQE in most cases is higher than the monochromatic value at 59.5 keV which is usually specified. The curves show a maximum at about 50 kVp and decrease again at lower kVp. This is due both to the absorption in the aluminum which becomes appreciable at lower energies (see figure 2), and the drop in the photo-electric absorption cross sections just below the K-absorption edge of Cs (36 keV) and I (33 keV).

**B. Rms method**

Another method is also frequently used for the determination of the DQE. This so called "rms method" measures the noise in the output image with an rms voltmeter and compares this to the noise in the X-ray beam determined by placing the thick reference crystal in the beam and measuring the rms noise at its output.

The noise amplitude determined this way is however not uniquely defined, but depends on the bandpass filter of the rms voltmeter. Since, by definition, the DQE is proportional to the ratio  $(noise_{in}/noise_{out})^2$  this would not be a problem, if both noise<sup>in</sup> and noise<sup>out</sup> vary by the same factor if the bandpass filter cut-off frequency is changed. Then their ratio would remain unchanged, and the measurement of the DQE would be frequency independent.

Unfortunately this is not the case. Indeed the input noise is generally measured with a fast NaI:TI reference crystal and since the quantum noise is essentially "white noise" its amplitude does not change with the frequency. The output noise on the contrary is greatly influenced by the lag of the P20 output phosphor which has a much slower response, and its magnitude decreases with increasing frequency. As a result the DQE measured by this method increases significantly when the frequency of the rms bandpass filter is increased.

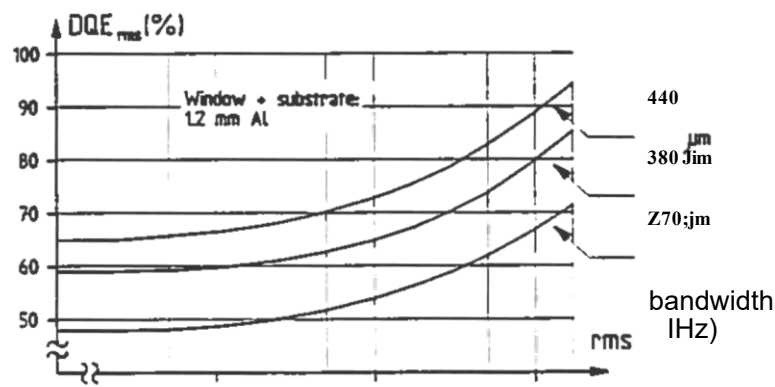


Figure 16 : Variation on the DQE<sub>rms</sub> with bandpass filter for different thicknesses of the CsI layer.

Figure 16 shows this variation of the  $DQE_{rm}$ , with the cut-off frequency of the bandpass filter. At very low frequencies ( $< 0.1$  Hz) the values measured with the rms method become identical to those obtained with the pulse counting method. Such very low cut-off frequencies are however very impractical since they require extremely long measuring times, and therefore are never used.

Typically used cut-off frequencies are 1.7 and 17 Hz. At these values the measured DQE is already significantly higher than the true zero frequency value, and at about 30 Hz the value would even exceed 100 percent. For these reasons the rms method should be progressively abandoned in the near future and, if still used, the employed cut-off frequency of the filters should be clearly indicated. Table 4 below shows a comparison of the DQE values obtained with different methods for some typical values of the CsI layer thickness.

	DQE (IEC)	DQE <sub>1.7</sub> (1.7 Hz)	DQE <sub>17</sub> <sup>TM</sup> (17Hz)
270 pm CsI	48	56	70
380 pm CsI	59	67	85
440 pm CsI	65	75	95

Table 4 : DQE values at 59.5 keV obtained with different measuring methods. The relative density of the layers is approximately 0.85. Total input window and substrate thickness : 1.2 mm aluminum.

### III. 4 Modulation Transfer Function

The spatial resolution of the image intensifier has a determining impact on the resolution of the final image obtained on film, or with high resolution TV cameras. Indeed, the high quality lenses and films available today have resolving powers which substantially exceed those of image intensifiers, and high resolution pick-up tubes, such as primicons, saticons or plumbicons have resolving powers which are generally also higher.

The resolving power is best described by the modulation transfer function (MTF), which gives the frequency dependence of the contrast transfer response for a sinusoidally modulated input signal.

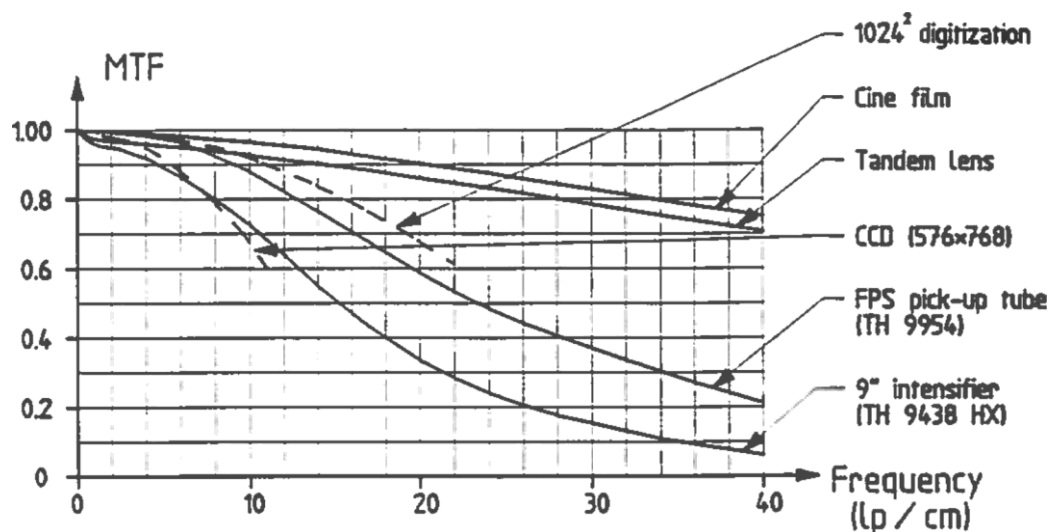


Figure 17 : MTF comparison of the various components in a high resolution 9" imaging chain.

Figure 17 shows a comparison between the center MTF's of various components in a typical state-of-the-art 9" imaging chain. All frequencies are converted to the entrance plane of the image intensifier and are directly comparable. Moreover, because of its multiplying properties, the MTF of the total system can be directly obtained by multiplication of the MTF curves of the individual components.

As can be seen, even a high resolution 9" image intensifier such as TH 9438 HX has a resolving power in the normal mode which is lower than that of a high quality pick-up tube. The MTF of the pick-up tube may however be further degraded by the MTF of the video amplifier (i.e. its bandpass) and the TV monitor, and generally the MTF of the complete video chain will be lower.

This is particularly true if the TV signal is digitized. Figure 17 shows the effect of a 1024 x 1024 digitization on the MTF of the TV signal. The loss of resolution above 10 lp/cm due to the digitization is non negligible and more important than the loss due the optics. Part of this loss will however be recovered by the powerful image processing techniques that become possible once the image is digitized, such as contour enhancement or grey scale windowing. The figure also shows the loss in MTF produced by a state-of-the-art CCD (450.000 pixels) when coupled to a 9" image intensifier. Due to the limited number of pixels, the MTF of the TV signal becomes severely truncated and will be insufficient for most high end applications.

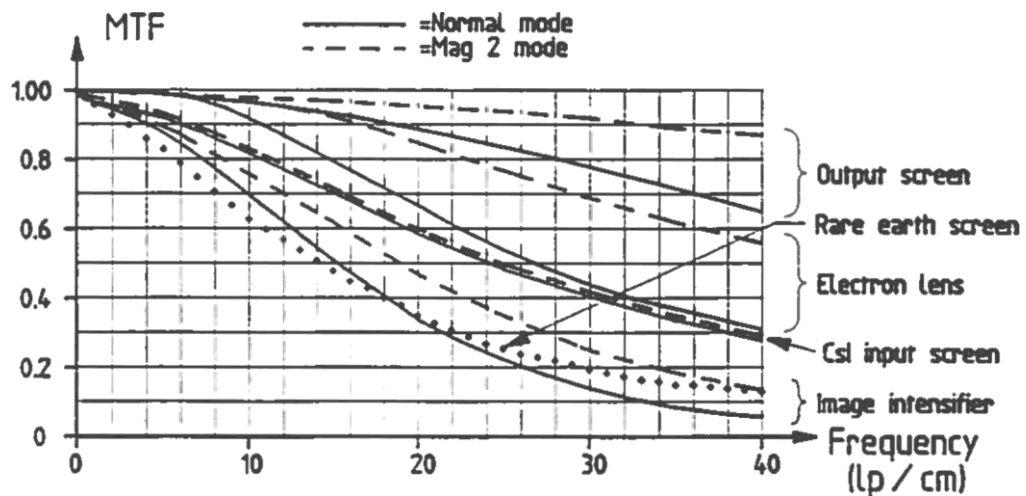


Figure 18 : MTF contributions of the different components in a 9" image intensifier.

Figure 18 shows the decomposition of the MTF of the 9" image intensifier itself. The individual contributions of the input screen, the electron lens and the output screen are shown both in the normal and in the MAG 2 mode of operation. The MTF of a typical medium speed rare-earth screen-film combination is also shown for comparison.

The figure illustrates the superior MTF characteristics of the CsI screen compared to conventional rare-earth screens. The CsI layer however remains the limiting component inside the image intensifier, especially when the magnifying modes are used. The increase in the MTF of the electron lens in the magnifying mode is due to the higher electric fields at the photocathode (section II.3) and the increase in the MTF of the output phosphor is due to its higher magnification ratio with respect to the entrance plane.

The small initial drop in the MTF curves at very low frequencies (below 1 lp/cm) is called the low frequency drop (LFD) and is due to the long range veiling glare. Various mechanisms are responsible for the veiling glare of image intensifiers : the scattering of X-rays at the input window, the backscattering of X-rays and light against the electrodes inside the tube, and the light reflections in the output window.

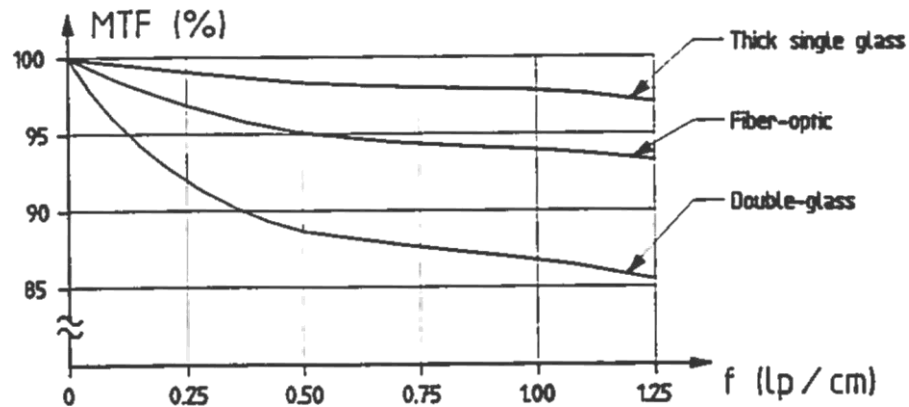


Figure 19 : Magnified view of the low frequency drop in the MTF curve for different type of image intensifiers.

Figure 19 compares the LFD of various image intensifiers with different output window structures. The multiple light reflections in the double glass output window structure shown in figure 8-a produce a LFD of about 13 percent, against only 6 percent for a fiber-optic window (figure 8-c). For a thick single glass output window (figure 8-d) the LFD becomes negligibly small.

Today, sophisticated measuring equipments exist which directly measure the MTF of image intensifiers including the LFD. Other methods exist however in which the MTF is normalized to unity at some arbitrary low frequency. In such measurements the veiling glare should be measured independently and the MTF should be corrected accordingly.

Although the MTF fully describes the spatial resolution characteristics of an imaging device, its resolving power at very low and at very high frequencies is often expressed by other parameters : the resolving power at very low frequencies, which only depends on the long range veiling glare, is often described by the contrast ratio and the limit of high frequencies is usually expressed in terms of limiting resolution. Both parameters will be described in the following sections.

### III. 5 Limiting spatial resolution

Traditionally the resolving power is also very often expressed in terms of limiting spatial resolution, which is defined as the highest number of rectangular space and bar combinations per unit length that can still be observed as separate entities.

This method has found wide spread applications because it requires only very simple test equipment : a template with an X-ray opaque space-and-bar pattern and a binocular for viewing the output image.



The major drawback of this method is its subjectivity since it relies upon human observation and between various observers important discrepancies may be found. The limiting spatial resolution as determined by an experienced observer corresponds to a contrast modulation of about 2 percent and therefore in principle the limiting resolution can be obtained from the MTF curve.

However, since MTF curves are relatively flat in the high frequency range, such measurements will generally not provide a better precision than the direct visual determination.

According to NEMA standard XR 11, the limiting spatial resolution should be measured with lead patterns of at least 100  $\mu\text{m}$  thickness for frequencies below 50 lp/cm and of at least 50  $\mu\text{m}$  thickness above 50 lp/cm. The radiation quality should be 50 kVp without any additional filtration. Measured this way the limiting spatial resolution of X-ray image intensifiers varies today typically between 35 and 55 lp/cm in the normal mode of operation. In the magnifying modes of operation the resolving power increases significantly, and limiting resolutions of more than 70 lp/cm can be achieved. Similarly, the resolving power will increase when larger output image diameters are used. This however occurs at the expense of the conversion factor (see section III. 2) and may become prohibitive in the magnifying modes of operation.

### III. 6 Contrast ratio

Like the low frequency drop (see section III.4) the contrast ratio is a measurement of the veiling glare of image tubes, but there exists no simple mathematical relationship between both parameters.

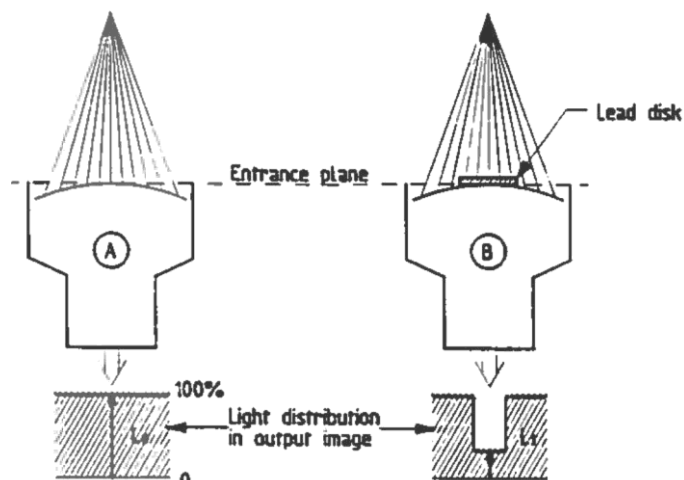


Figure 20 : Definition of the contrast ratio



The definition of the contrast ratio is illustrated in figure 20. The contrast ratio is defined as the ratio between the luminance in a given point of the output image (generally the center) if no object is present in the entrance plane (A), and the residual luminance at the same point if the corresponding point in the entrance plane is covered with an X-ray opaque disk under exactly the same exposure rate (B). A contrast ratio of 20 :1 means that the residual light level is 5 percent, whereas a contrast ratio of 33 :1 corresponds to a residual light level of 3 percent.

Although a contrast ratio of 33 :1 seems to suggest a significant improvement with respect to a contrast ratio of 20 :1, the corresponding reduction in veiling glare is only 2 percent. Such a difference is much smaller than the contrast reduction due to X-ray scatter in the patient, which in any case produces an undesired background signal of 5 to 20 percent depending on the patient thickness and the quality of the anti scatter grids used. For not too large values the 1/C ratios are additive and for example with 10 percent residual X-ray scatter the contrast ratio in the final image will be 6.7 :1 and 7.7 :1 for image intensifiers with a 20 :1 and 33 :1 contrast ratio respectively.

Hence the difference in contrast in the final image (which may even be further attenuated by the contrast loss in the lenses or TV camera) is much smaller than the contrast values of the image intensifier itself suggest, and generally contrast ratios of the image intensifier much higher than 20 :1 do not really provide a significant improvement in the final image.

In fact a much more important matter is to maintain a high contrast ratio irrespective of the size of the lead disk, and in particular for very small objects.

Traditionally the contrast ratio has been defined as the so called 10 percent contrast ratio. This means that the residual light output is measured with a lead disk that has a surface of 10 percent of the useful entrance field of the image intensifier. When the size of the disk decreases, more X-rays and light will be scattered, and as a result the contrast ratio will always decrease when the size of the lead disk decreases. The small detail contrast ratio, measured with a 10 mm lead disk, has recently been introduced and gives a more representative indication for the contrast of clinically relevant details.

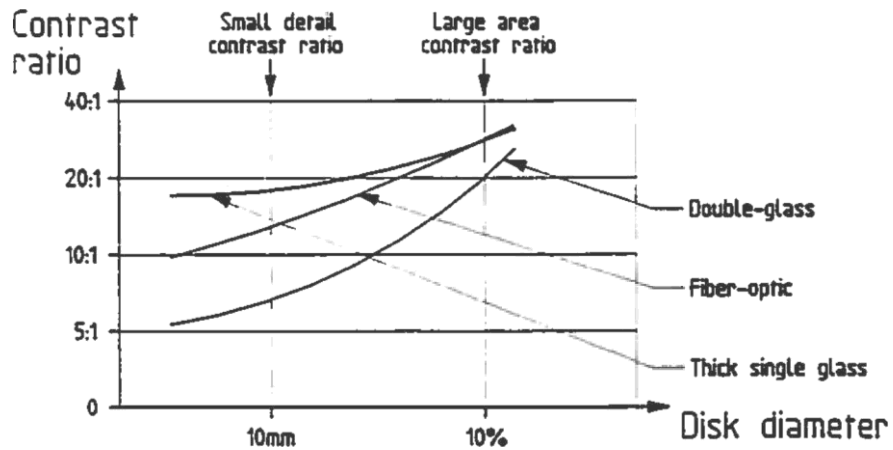


Figure 21 : Variation of contrast ratio with object size.

Figure 21 shows the typical dependence of the contrast ratio on the disk diameter for image intensifiers with various output window structures. The multiple light reflections in the double glass output window (see figure 7-a) are clearly seen to affect the contrast of small objects. The light scattering between different fibers in a fiber-optic output window (figure 7-c) depends strongly on its quality, its shape and its thickness, but generally has a non negligible impact on the small detail contrast ratio. In the thick output window (figure 7-d) most light reflections are suppressed. Since the residual veiling glare due to X-ray and light scatter inside the tube increases much less with decreasing disk size, image intensifiers manufactured with such windows provide excellent contrast for small details irrespective of the object size.

The contrast ratio is usually specified at 50 kVp without additional filtration, but it depends on the X-ray spectrum. Figure 22 shows the typical variation of the contrast ratio as a function of the X-ray tube voltage with 22 mm of Al total filtration. At higher kVp the contrast decreases due to increased X-ray and light diffusion inside the image intensifier.

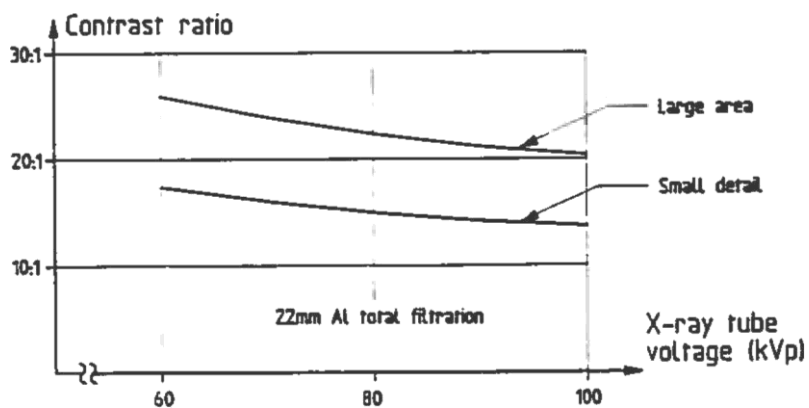


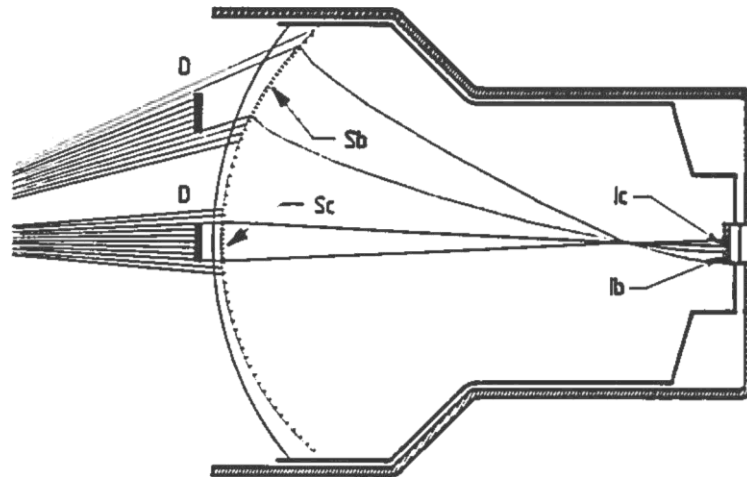
Figure 22 : Variation of contrast ratio with X-ray tube voltage.

III. 7 Image distortion

The geometric shape of the final image produced by an image intensifier chain is never perfectly proportional to the shape of the corresponding object. This phenomenon is called image distortion and is principally due to the image intensifier itself. Two types of distortion should be distinguished : circular symmetric, geometric distortion and asymmetric, often called S-distortion.

\* Geometric distortion

Geometric distortion is due to the fact that the X-ray image is projected onto a curved surface. As can be seen in figure 23 an object O in the entrance plane produces a larger image at the border ( $S_b$ ) than at the center ( $S_c$ ) of the input screen. This (positive) distortion is related to the geometry of the input screen and the position of the X-ray source and is therefore called geometric distortion.



local magnification at border =  $M_b = \frac{I_b}{S_b} = \frac{S_c}{D}$

local magnification at center =  $M_c = \frac{I_b}{S_c} = \frac{S_b}{D}$

differential distortion =  $M_b/M_c - 1$

$$\frac{I_b}{S_b} \cdot \frac{S_b}{D} = \frac{I_b}{D}$$

$$\frac{I_b}{S_c} \cdot \frac{S_c}{D} = \frac{I_b}{D}$$

Figure 23 : Definition of geometric image distortion.

An electron lens designed in such a way that it has a negative distortion (i.e.  $I_b/S_b < I_c/S_c$ ) will partially compensate for the positive distortion due to the curvature of the input screen and hence attenuate the total distortion in the output image. This is illustrated in figure 24 for a typical 12" image intensifier in the normal mode of operation. Although some attenuation can indeed be obtained by an appropriate electron lens design, the total distortion remains largely positive and produces the characteristic pin cushion shape of a squared object.

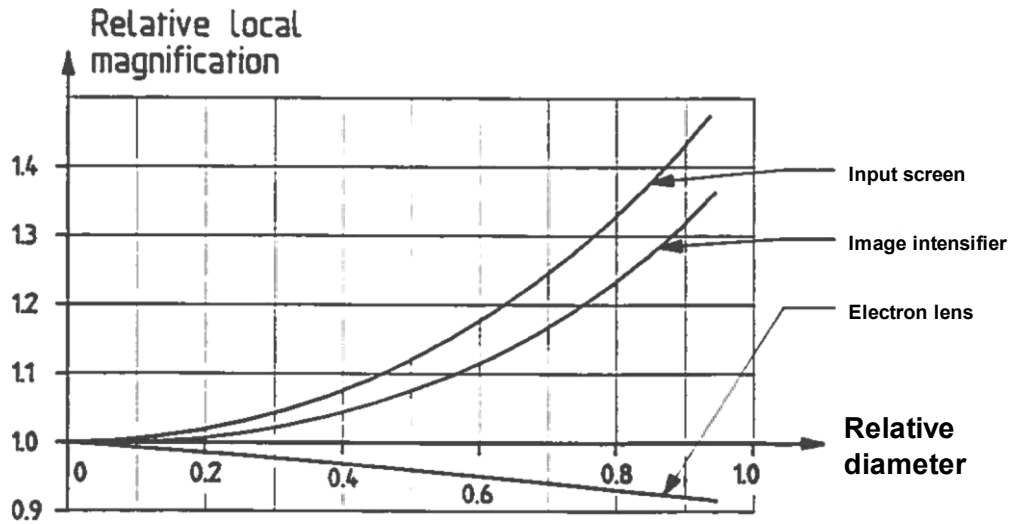


Figure 24 : Compensating effect of the electron lens on the geometric distortion.

The differential distortion is generally specified at 90 percent of the useful entrance field diameter. Typical values are between 10 and 20 percent for small field of view image intensifiers and between 20 and 30 percent for larger field of view tubes.

The integral distortion is defined as the integrated ("averaged") value of the differential distortion between the center and 90 percent diameter, and is always much smaller than the differential distortion. Values of the integral distortion between 5 and 10 percent are typical.

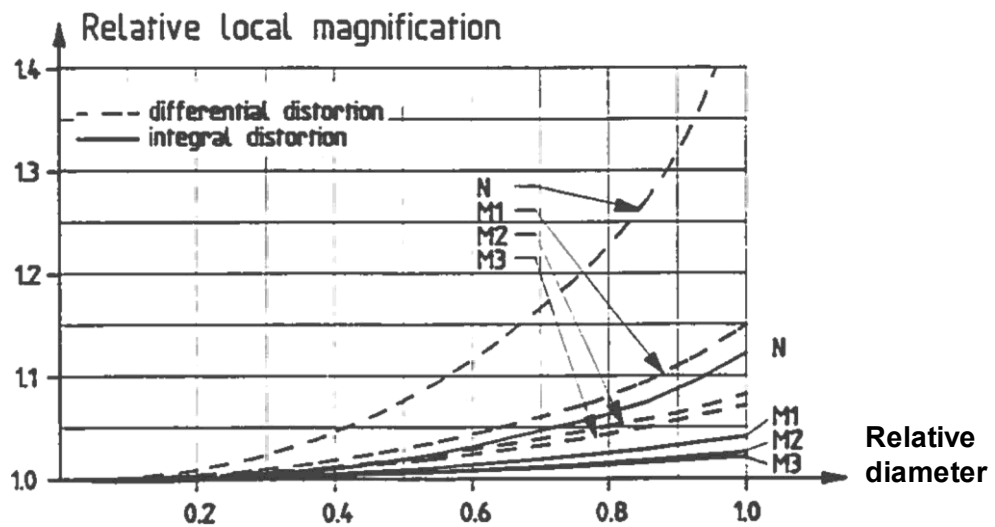


Figure 25 : Variation of the integral and differential distortion in the magnifying modes.

The geometrical distortion is only important in the normal mode of operation and rapidly vanishes in the magnifying modes (see figure 25). Moreover sophisticated TV cameras are now becoming available that enable one to correct almost completely for the image distortion in an all-electronic imaging chain.

\* S - distortion

The other type of distortion is called S-distortion because of the characteristic S-shaped image of a rectilinear object. This phenomenon is due to stray magnetic fields like the earth magnetic field or those emitted by surrounding equipment. Indeed, the electron trajectories are very sensitive to a magnetic field, which causes the image to rotate with an angle that depends on the radius. The earth magnetic field varies between 0.3 and 1 Gauss depending on the location, and may cause appreciable S-distortion in the larger field of view tubes. For this reason most image intensifiers have an incorporated mu-metal shield which protects the electron lens against external magnetic fields and thus reduces S-distortion as much as possible.

For maximum efficiency such mu-metal shieldings should completely surround the tube including the entrance plane. Unfortunately mu-metal alloys, which have to be highly permeable, contain relatively heavy metals like Fe, Ni or Co, and even thin sheets already show significant X-ray absorption. Therefore in most cases no mu-metal protection is present at the entrance, but by extending the outer cylindrical shielding at maximum in the direction of the X-ray source, an acceptable distortion level is generally achieved.

Obviously care should be taken to avoid the presence of magnetic field sources, like magnetic resonance equipment in the vicinity of the image intensifier. This is particularly true for alternating field sources such as heavy-duty transformers, which may cause an appreciable loss of resolution.

III. 8 Brightness non-uniformity

When an image intensifier is irradiated with a perfectly uniform exposure rate in the entrance plane, the luminance should also be constant over the whole output image area. In reality, due to the geometrical distortion, this is never completely true. The output luminance is a flux density (see section III. 2) and hence decreases when the local magnification increases. Although an adequate design of the scintillator-photocathode structure may partially compensate such variations, the brightness in the output image will generally be about 10 to 20 percent lower at the border (90 percent diameter) compared to the value at the center. Since this brightness fall-off is mainly related to the distortion, it is only significant in the normal mode of operation and becomes negligibly small in the magnifying modes. Typically the brightness non-uniformity is divided by two, each time the zoom is increased and in the highest magnification mode the residual variation is only a few percent.



Since the brightness non-uniformity is related to the differential absorption of X-rays in the CsI layer it depends strongly on the quality of the radiation. The brightness non-uniformity always increases when lowering the kVp, and typically doubles when going from 100 kVp to 50 kVp. Usually its measurement is made at about 75 kVp with the same radiation quality used for the measurement of the conversion factor (see section III.2).

### III. 9 Lifetime

It is very difficult to have a general answer to an often asked question : what is the life of an X-ray image intensifier ? Indeed the answer very much depends on the type of application and the frequency of use. In normal use the life of the tube typically varies from 6 to more than 10 years. In very intensively used equipment like cath-lab's for example, the tubes are replaced more frequently, typically between 3 and 6 years.

In fact almost all electro-optical performances (DQE, contrast, resolution, distortion) are determined by design and will not vary throughout the life of the tube. Only the conversion factor will progressively decrease and ultimately become unacceptably low. The minimum acceptable value is not readily definable however, but depends on the application (see section III.2).

Two mechanisms are responsible for this fall-off of the conversion factor :

Firstly, the photocathode will progressively lose some of its sensitivity. The photocathode is a very thin layer of only about 20 nm thickness and is therefore very sensitive to surface contamination. Although most image intensifiers have incorporated passive, or even active getter pumps, the vacuum inside the tube is never perfect and will contaminate the photocathode at a very slow rate. This decrease is most important in the beginning (typically between 5 and 10 percent in the first year) and will progressively slow down to a few percent per year. The loss of photocathode sensitivity in time is independent of the photocathode current and will occur no matter if the image intensifier is used or not.

Secondly, the output screen and, to a lesser extent, the input screen will lose some of their conversion efficiency. This process however only occurs when the tube is in operation and the loss is roughly proportional to the total received amount of X-ray dose. Typically the conversion factor fall-off is between 5 to 15 percent per integrated dose of about 10 Gy (1000 R) in the first years and will become less afterwards.

#### **IV. CONCLUSION**

State-of-the-art X-ray image intensifiers, although significantly improved in the past years, very often remain the most critical component in high quality fluoroscopic or fluorographic imaging chains. Today however no alternative solutions exist which offer comparable performances in image quality, dose reduction, speed and cost efficiency. Scanning devices using linear or multilinear X-ray detectors provide excellent image quality with improved contrast due to their insensitivity to X-ray scatter, but are incapable of working at fluoroscopic speeds of 30 images/sec. or more. The development of two dimensional solid state detectors is related to the progress made in large area semiconductor technology, and devices capable of producing real time images of large dimensions will not be available for many years. Other imaging modalities, such as computed tomography or magnetic resonance either lack resolution or speed and do not offer the same accessibility to the patient.

Therefore X-ray image intensifiers will continue to be used extensively in the years to come and an important effort is maintained to improve their performances. In particular, the further improvement of resolution together with the high resolution pick-up tubes that now are available and the advent of megapixel CCD's will make it possible in the near future to produce real time electronic images with a quality comparable to those obtained with conventional screen-film combinations, at consirably lower dose.

#### Acknowledgments

The author would like to thank J.M. D6on for the calculation of the X-ray spectra and many fruitful discussions. P. Fessou and D. Barjot, who carried out most of the measurements are also gratefully acknowledged.

#### References

The X-ray spectra used for the various absorption and transmission curves were calculated from the Catalogue of Spectral Data for diagnostic X-rays published by R. Birch, M. Marshall and G.M. Ardran of the Hospital Physicists' Association, 1979.